Journal of Applied Polymer Science

High flux nanofibrous composite microfiltration membrane prepared by melt blending extrusion: Application in liquid filtration

Dandan Xu, Keying Zhu, Xiaoting Zheng, Ru Xiao
State Key Laboratory for Modification of Chemical Fibers and Polymer Materials, College of Materials Science and Engineering, Donghua University, Shanghai, 201620, People's Republic of China
Correspondence to: R. Xiao (E-mail: xiaoru@dhu.edu.cn)

ABSTRACT: High flux PP/EVOH nanofibrous composite microfiltration membrane (P/E-NCMM) based on polypropylene (PP) (575 nm) and polyethylene-*co*-polyvinyl alcohol (EVOH) nanofibers (248 nm) with low operation pressure for liquid filtration was fabricated by melt blending extrusion. PP nanofibers as the scaffold played a supporting role, and EVOH nanofibers filled in the PP nanofibers network structure narrowed the pore size and improved the wettability. Taking advantages of PP and EVOH nanofibers, the nanofibrous composite membrane created fascinating features for liquid filtration. The experimental results showed that the P/E-NCMM had high average pure water flux at low operating pressure. The P/E-NCMM with 30 wt % PP nanofibers showed high water flux [450.9 L/(m^2 h)] even at very low feeding pressure (0.05 MPa) with above 95% retention for TiO_2 suspension. The results indicated that the P/E-NCMM prepared by this method had great potential for the application in liquid filtration. © 2016 Wiley Periodicals, Inc. J. Appl. Polym. Sci. **2016**, *133*, 43585.

KEYWORDS: fibers; membranes; liquid filtration

Received 8 September 2015; accepted 23 February 2016
DOI: 10.1002/app.43585

INTRODUCTION

To our knowledge, membrane separation technology has been broadly used in chemical industry, light industry, electronics,[1] textile, metallurgical industry,[2] especially in sewage treatment fields.[3] With the help of external energy and chemical potential driving, membrane separation technology can achieve the separation of mixing liquid or gas.[4] Polymer membrane materials play a very important role in this technology, widely used in all kinds of membrane separation process.[5]

Nanofibrous membrane has some good performance, such as high porosity, large specific surface area, good biocompatibility, and low flow resistance. Recently, it has been found application in many areas, including the separator of lithium-ion batteries,[6,7] sensors,[8,9] filtration,[10–12] dye-sensitized solar cells, tissue engineering,[13] adsorption of heavy metal pollutants and dyes from wastewater,[14,15] and so on. As a kind of separation membrane, it has also been used in microfiltration,[16] ultrafiltration,[17] nanofiltration,[18] reverse osmosis, and electroanalysis.

To date, many methods have been developed to prepare nanofibers, including electrospinning,[19] polymerization, melt blowing,[20] cold drawing,[21] centrifugal force spinning, phase separation,[22,23] and melt blending extrusion.[24,25] Most polymer resins used for this purpose are thermoplastic polyolefins or polyesters, which can be melted and reprocessed. The melt blending extrusion method for preparing various kinds of thermoplastic polymer nanofibers is environment friendly, high efficiency, versatility, and continuous.[26,27] Recently, the fabrication of fibrous membranes with large specific surface area and high porosity via melt blending extrusion has been widely studied.[28–30] In the melt blending extrusion process, the dispersed phase is stretched into nanofibers, then the thermoplastic polymer nanofibrous membranes are obtained after the matrix phase is removed.

In this study, polypropylene (PP) and polyethylene-*co*-polyvinyl alcohol (EVOH) nanofibers were prepared from PP/cellulose acetate butyrate (CAB) and EVOH/CAB, immiscible polymer blends, by the melt blending extrusion process. Then PP/EVOH nanofibrous composite microfiltration membrane (P/E-NCMM) was prepared via the airflow deposition process. The properties of P/E-NCMM including the surface morphology, apparent density, porosity, wettability, pore size distribution, specific surface area, water flux, and filtration performance were investigated. Based on the properties of nanofibrous membranes, the P/E (30/70)-NCM was selected as the most favorite one, which could be used in filtration field.

Additional Supporting Information may be found in the online version of this article.

EXPERIMENTAL

Materials

Poly(ethylene-*co*-vinyl alcohol) (EVOH, Model: ET3803) with 38 mol % ethylene was supplied by Nippon Gohsei, Japan. Polypropylene (PP, Model: Y2600T) was supplied by Sinopec Shanghai Co., Ltd., China. Cellulose acetate butyrate ester (CAB, Model: 381-20, butyryl content 37 wt %, acetyl content 13.5 wt %, and hydroxyl content 1.8 wt %) was purchased from the Eastman Chemical Company (The United States). Titanium dioxide 99.8%, 100 nm, anatase, hydrophilic, was purchased from Aladdin (Shanghai, China).

Preparation

PP and EVOH nanofibers were prepared according to a previously published procedure.[31] EVOH was dried in electric heating air-blowing drier for 24 h at 80 °C and the other materials were dried in vacuum drying oven for 24 h at 100 °C before melt blending. PP/CAB and EVOH/CAB blends with the weight ratios of 20/80 were fed into the co-rotating twin-screw extruder ($D = 16$ mm, $L/D = 40$, EUROLAB16, Thermo-Haake Co.) with a screw speed of 50 rpm and melting zone temperature were 200–225 °C for EVOH/CAB and 190–230 °C for PP/CAB. The blends were extruded by a take-up device and water-cooled to room temperature. Then the extrudants were immersed in acetone via a Soxhlet extractor at room temperature for 24 h to remove CAB from the blends. After removing the matrix phase CAB, PP, and EVOH nanofibers were obtained for the following preparation of P/E-NCM.

The prepared PP and EVOH nanofibers were mixed with the weight ratios of 10/90, 20/80, 30/70, 40/60, dispersed using a mechanical disintegrator for 30 s to obtain a consistent fiber suspension, and then a layer of the fibers was deposited onto a supporting PP nonwoven mat. After drying in a electric heating air-blowing drier for 5 min at 60 °C, the P/E-NCM with a controlled thickness was released from the supporting PP nonwoven mat.

The heat-treated P/E-NCM was prepared by drying in a vacuum drying oven for 10 min at 150 °C.

Measurement and Characterization

Morphology and Structure. The morphology of P/E-NCM was characterized using scanning electron microscopy (SEM, S-3000N, Hitachi, Ltd., Japan). The diameter of nanofibers was tested by image analysis. The number averaged diameter distribution of nanofibers was selected in this study. The diameter distribution and averages of 100 nanofibers were also obtained by image analysis.

The number averaged diameters were calculated as the following eq. (1):

$$D_N = \frac{\sum N_i D_i}{\sum N_i} \tag{1}$$

where D_N is the number averaged diameter and N_i is the number of nanofibers with the diameter of D_i.

The apparent density and porosity of NCM were calculated from eqs. (2) and (3).[32] Water contact angle measurement with water volume 3 μL was performed using a contact angle goniometry (OCA 40 Micro, Dataphysics Ltd., Germany) to evaluate wettability of NCM. The specific surface areas were obtained by the specific surface area and pore size analyzers (Autosorb-1 Quantachrome instrument, The United States). The pore sizes and pore size distributions of NCM were examined using a capillary flow porometer (CFP-1100AI, Porous Materials Inc., The United States). The above tests were repeated five times and the average value was taken.

$$\text{NCM apparent density } (\text{g/cm}^3) = \frac{\text{NCM mass (g)} \times 10}{\text{NCM thickness (mm)} \times \text{NCM area (cm}^2)} \tag{2}$$

$$\text{NCM porosity} = \left(1 - \frac{\text{apparent density of NCM } (\text{g/cm}^3)}{\text{bulk density of raw material } (\text{g/cm}^3)}\right) \times 100\% \tag{3}$$

Water Flux. A crossflow filtration device (self-made) was used to measure the pure water flux of corresponding membrane. The effective membrane area was 3.17 cm^2. The membranes should be prepressed with inlet pressure 0.05 MPa for 10 min before flux test. This experiment was repeated five times and the average value was taken.

The pure water penetration flux was defined as the following eq. (4):

$$J = \frac{Q}{A \cdot T} \tag{4}$$

where J is the pure water flux of corresponding membrane (L/m^2 h), Q is the volume of permeate water (L), A is the effective area of the membrane (m^2), and T is the permeation time (h).

Filtration Performance. In order to evaluate the filtration properties of NCM, 0.5 wt % TiO_2 (particle diameter: 0.1–1 μm) suspension was prepared. The separation test was carried out at a preset pressure using wetted NCM. The pure water flux was first tested, followed by the separation of TiO_2 suspension. These tests were repeated three times and the average value was taken. Since the TiO_2 dispersion used was stable and the particle size distributions of TiO_2 nanoparticles were very narrow, the effect of diameter variance on the adsorption intensities measured for different samples with UV–Vis spectrometer could be offset. The concentrations of TiO_2 suspension before and after filtration were measured by a UV–Vis spectrophotometer (Lambda 35 PerklinElmer, The United States) with wavelength between 300 and 600 nm. The rejection ratio was calculated by the following eq. (5):

$$\text{Rejection} = \frac{C_f - C_p}{C_f} \tag{5}$$

where C_f is the concentration of prepared TiO_2 solution before filtration and C_p is the concentration of TiO_2 solution after filtration.

Membrane Fouling. The interactions of particle–particle and particle–membrane induce particle aggregation in solution or on surfaces and affect permeation rates through pore plugging, pore narrowing, and cake deposition, which are thought to be the membrane fouling.[33,34] The resistance-in-series model was

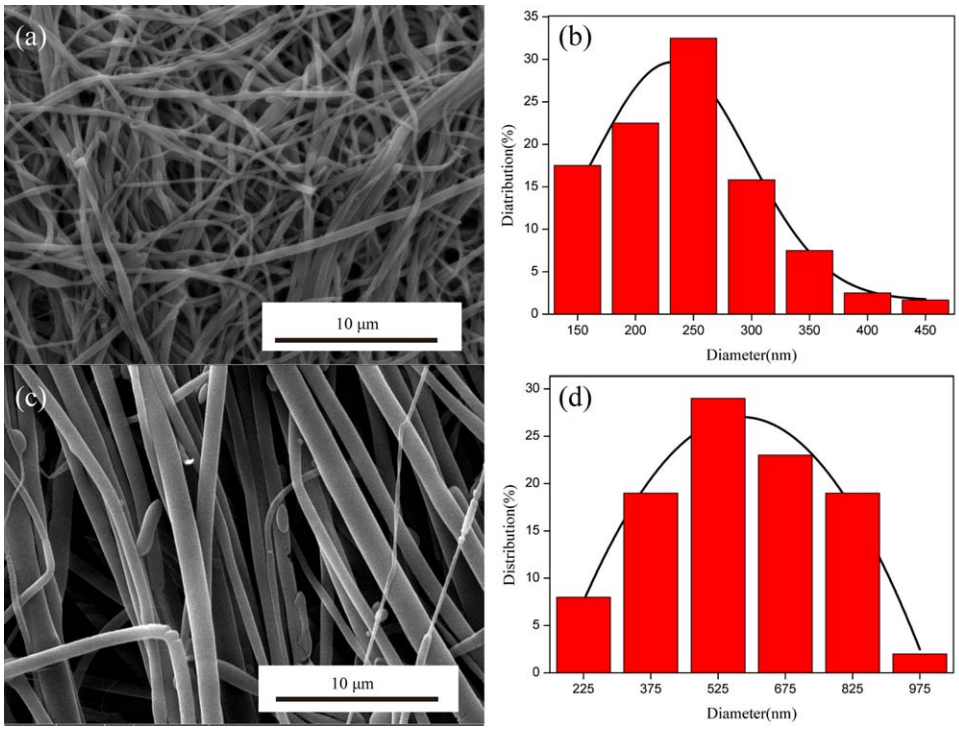

Figure 1. (a) SEM image of EVOH nanofibers. (b) Diameter distribution of EVOH nanofibers. (c) SEM image of PP nanofibers. (d) Diameter distribution of PP nanofibers. [Color figure can be viewed in the online issue, which is available at wileyonlinelibrary.com.]

used to analyze membrane fouling resistances, which described the permeate flux-transmembrane pressure (TMP) relationship over the entire domain of pressure. Based on this model, the permeate flux on the applied TMP was described by Darcy's law [eq. (6)][35]:

$$J_v = \frac{1}{A}\frac{dV}{dt} = \frac{\Delta P}{\mu R_t} = \frac{\Delta P}{\mu\left(R_m + R_c + R_{a+p}\right)} \quad (6)$$

where J_v is the permeate flux (L/m^2 h), V is the total volume of permeate (L), A is the membrane area (m^2), ΔP is the TMP (Pa), and μ is the dynamic viscosity of permeate (Pa s). Total membrane resistance R_t (m^{-1}) is composed of intrinsic membrane resistance R_m (m^{-1}), adsorption and pore blocking resistances R_{a+p} (m^{-1}), and cake layer resistance R_c (m^{-1}). This experiment was repeated three times and the average value was taken.

RESULTS AND DISCUSSION

Morphology and Structure

The morphology and size distribution of PP and EVOH nanofibers are shown in Figure 1. The diameter distribution of EVOH nanofibers was in the range of 150–450 nm, with the average diameter 248 nm [Figure 1(b)]. While PP nanofibers diameter distribution was in the range of 225–975 nm, and the average diameter was 575 nm [Figure 1(d)]. The average diameter of PP nanofibers was significantly higher than that of EVOH nanofibers. Therefore, in the preparation of PP/EVOH nanofibrous composite membrane (P/E-NCM), PP nanofibers as the scaffold played a supporting role, and EVOH nanofibers would be filled in the PP nanofibers network structure. The specific surface area of nanofibers was beneficial to the functional modification of the fiber, and improved the function efficiency, which increased with fiber diameter reduced.

Because of the large specific surface area of prepared nanofibers, the nanofibrous membrane obtained from nanofibers also had large specific surface area. Table I was the data of specific surface area and pore size of PP and EVOH nanofibers. From the data shown in the Table I, EVOH nanofibers had the specific surface area of 20.65 m^2/g, which was larger than the PP nanofibers with specific surface area of 5.72 m^2/g. This was because the average diameter of EVOH nanofibers was significantly less than the diameter of the PP nanofibers, and the specific surface area of nanofibers was inversely proportional to the size of the fiber diameter.

Figure 2 showed the morphology of P/E-NCM with different components and heat-treated. As shown in Figure 2, nanofibers in P/E-NCM were shorter and disorder due to high shear mixer broken and scattered in the preparation process of P/E-NCM. It was clearly presented that PP nanofibers in PP nanofibrous membranes disperse uniformly [Figure 2(a)]. As shown in Figure 2(b), when PP and EVOH nanofibers dispersed with different components by high shear mixer, the coarse PP fibers

Table I. The Surface Area and Pore Properties Date of PP and EVOH Nanofibers

Sample	BET surface area (m^2/g)	Pore diameter (nm)
PP nanofiber	5.72	3.72
EVOH nanofiber	20.65	4.56

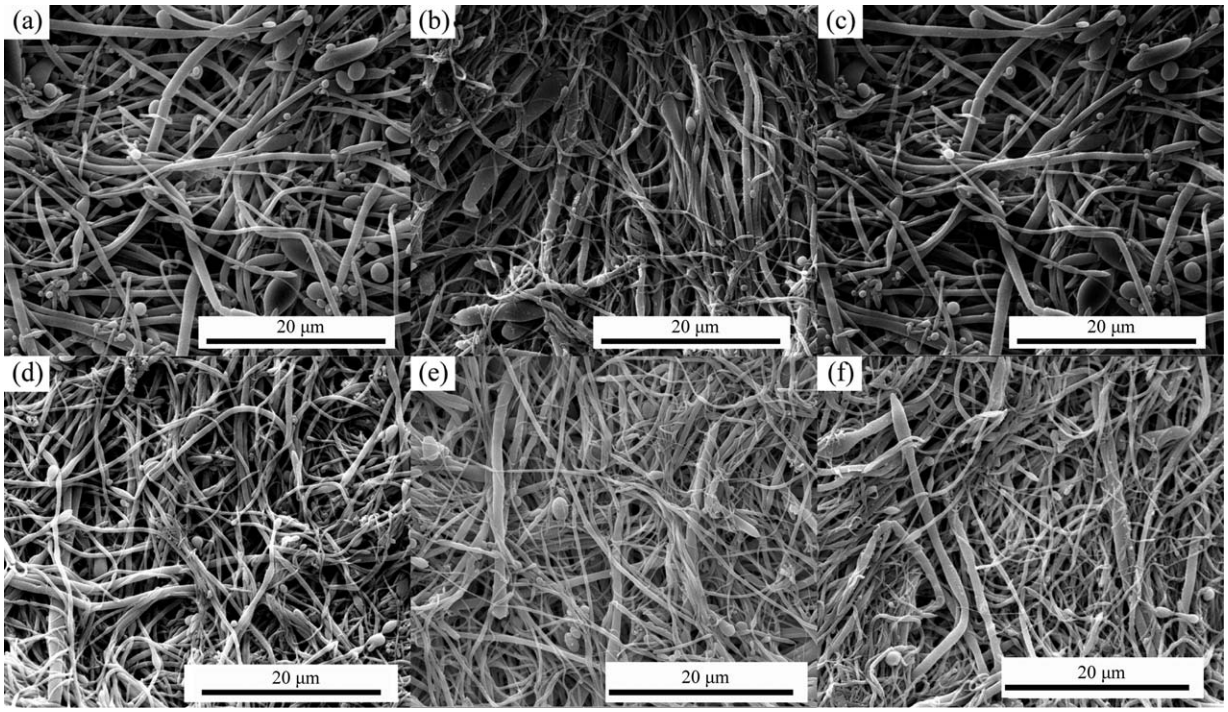

Figure 2. SEM image of surface morphology of P/E NCM, (a) 100/0, (b) 10/90, (c) 20/80, (d) 30/70, (e) 40/60, and (f) heat-treated 30/70.

formed a network and played a supporting role as a scaffold, while the thin EVOH nanofibers filled in PP fiber networks, and concentrated in the surface of P/E-NCM, leading to the formation of more small holes as shown in Figure 2(c). With the increasing of PP fibers, more coarse fiber support formed and the fine EVOH nanofibers had been completely filled in the PP fiber network structure. Figure 2(f) showed the heat-treated P/E(30/70)-NCM. As shown in the Figure 2(f), after heat treatment at 150 °C for 10 min, there were cross-linking points between the nanofibers due to the low melting point of EVOH and PP.

The porosity of porous materials refers to the ratio of pores and the total volume of porous materials. The ideal fiber filter materials should be able to filter all particles in the liquid with minimum pressure loss and the maximum pollutants capacity. However, this is incompatible. When the fineness of filter material is small, the pressure loss will increase and the pollutants capacity will decrease. There are many factors affecting the filtration performance of fiber filter material, such as fiber diameter, fiber surface smooth degree, as well as the shape of fiber cross-section. Therefore, in order to make the fiber filtration material has good filtration performance, which requires the nanofibrous membrane has a high porosity and appropriate pore size and pore size distribution.

Table II was the density, porosity and the contact angle of P/E-NCM with different components. As shown in Table II, with PP fibers increasing, the porosity of P/E-NCM increased, while the density decreased. This was possibly because PP fibers had relatively larger diameter, which played a supporting role in the process of NCM formation and tended to form scaffolds. With EVOH thin nanofibers filled in the PP fiber network structure, the large gap was divided into smaller voids, which increased the porosity of the NCM with more closely structure, and improved the fineness simultaneously. But the porosity of P/E-NCM decreased with high PP fibers contents as shown in Table II. It also could be seen that the porosity of the PP/EVOH (30/70)-NCM decreased after heat treatment, caused by the softening and crosslinking of nanofiber surface when heated, thus blocking or reducing the space between the fibers.

Contact angle is one of the important judgments for the surface wettability of membrane material. Generally speaking, the water contact angle of the material with good hydrophilic is less than 90°. The water contact angle of P/E-NCM with different components was shown in Figure 3, and the average contact angle was listed in Table II. As could be seen from Figure 3(a), the average contact angle of EVOH nanofiber membrane was the

Table II. The Apparent Density, Porosity, Contact Angle of P/E NCM with Different Blend Ratios

P/E NCM	Apparent density (g/cm^3)	Porosity (%)	Contact angle (°)
10/90	0.41	64	73
20/80	0.32	70	82
30/70	0.33	72	99
(30/70 heat-treated)	0.38	65	99
40/60	0.32	70	125

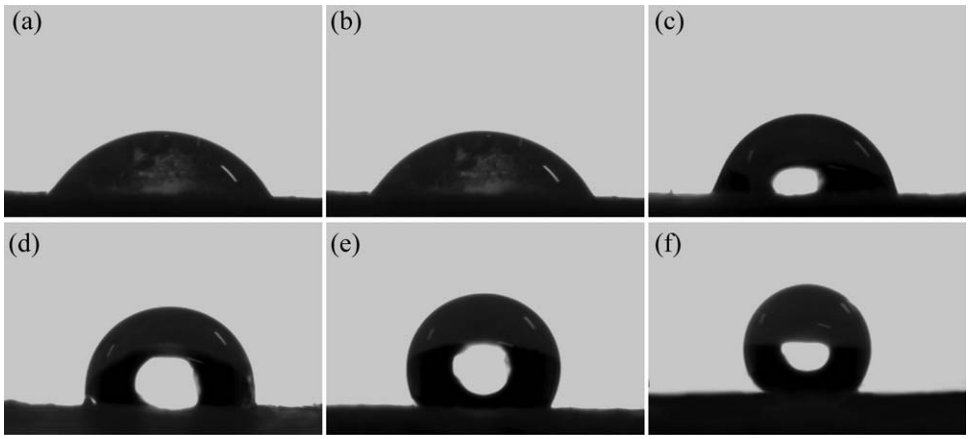

Figure 3. Water contact angle of P/E NCM with different blend ratios, (a) 0/100, (b) 10/90, (c) 20/80, (d) 30/70, (e) 40/60, and (f) 100/0.

minimum one with 67°, due to hydroxyl groups (—OH) in EVOH membrane surface. At the same time, it was clearly observed that the water contact angle increased with PP added in [Figure 3(b–f)], because of the lacking of polar groups in PP molecular structure. What's more, with the increasing of PP nanofibers content, the water contact angle of P/E-NCM increased. In this research, the wettability of membranes would affect their dispersion in water, which was used as the dispersion medium, thereby affecting the performance of the nanofiber composite membrane.

Pore Size and Pore Size Distribution

Pore size and pore size distribution are the important properties of membrane material and have tremendous influence on the membrane filtration performance. Therefore, it is necessary to study the factors for pore size and pore size distribution in the process of preparation and using of nanofiber membrane. The pore size and pore size distribution of this experiment mainly tested by bubble point method using capillary flow porometer, and the capillary flow porometer date of P/E-NCM with different component ratio was shown in Supporting Information Figure S1.

Figure 4 showed the pore size distribution of P/E-NCM with different component ratios. It was clearly shown that the aperture of NCM distributed in the range of 0.3–1.5 μm, which belonged to the range of microfiltration. Simultaneously, 90% was in the range of 0.3–1 μm with 10% PP fibers. With the increased of the content of PP fibers, pore size distribution of NCM became wider, the proportion of larger than 1 μm increased, but the membrane still within the scope of the microfiltration. Figure 4(e) showed the pore size distribution of heat-treated P/E (30/70)-NCM. It indicated that 80% pores of heat treatment membrane distributed in the range of 0.3–0.7 μm,

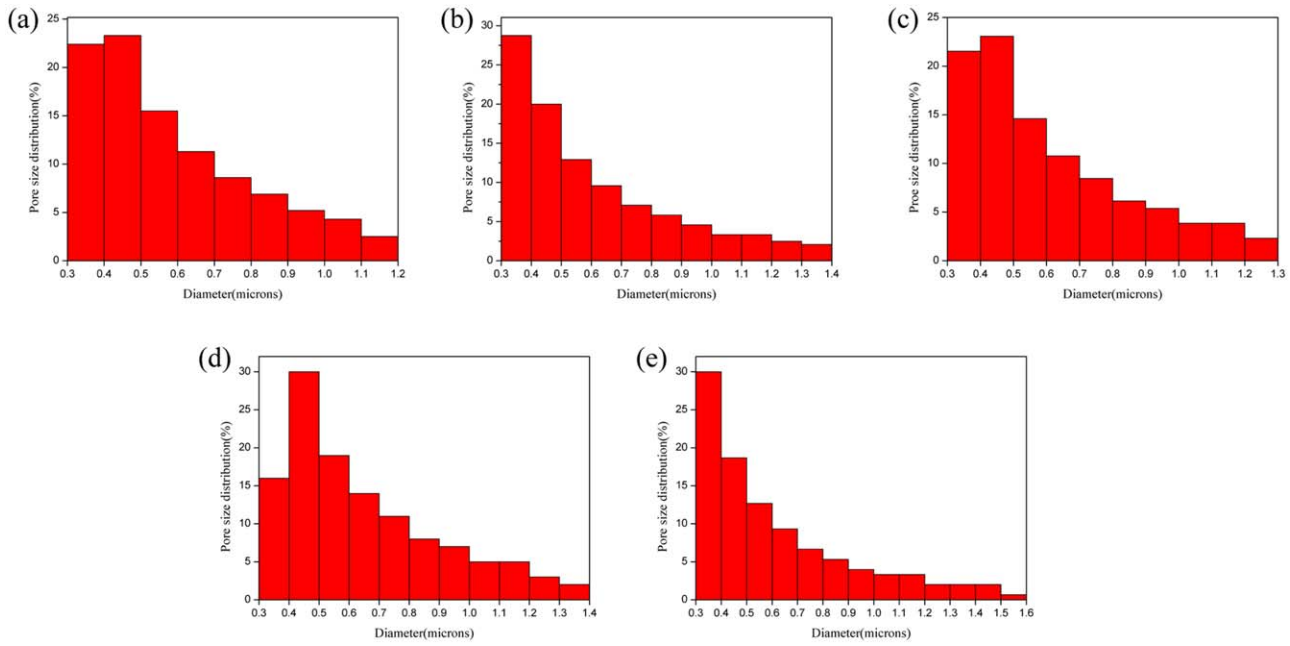

Figure 4. The histogram of pore size distribution of P/E NCM with different blend ratio, (a) 10/90, (b) 20/80, (c) 30/70, (d) 40/60, and (e) heat-treated 30/70. [Color figure can be viewed in the online issue, which is available at wileyonlinelibrary.com.]

Table III. The Pore Size Properties of All Kinds of P/E NCM with Different Blend Ratios

P/E NCM	Maximum diameter (μm)	Mean diameter (μm)	Minimum diameter (μm)
10/90	1.16	0.34	0.26
20/80	1.41	0.51	0.31
30/70	1.35	0.46	0.34
Heat-treated (30/70)	1.22	0.43	0.23
40/60	1.43	0.59	0.34

and the pore size distribution was more concentrated. Table III listed the aperture data of different component ratio of NCM, including the maximum, minimum and average pore size. As shown in the Table III, the average pore size of the P/E-NCM with different components were 340, 510, 460, 590, and 430 nm. It was noted that the adding of PP fibers increased the average pore size, while the heat treatment process reduced the pore size due to the compact, dense structure of membrane after the heat treatment.

Water Flux

The water flux of nanofiber membranes affects its performance and reflects its permeability. The water flux of five kinds of membranes was mainly discussed in this section, including the commercial cellulose ester microfiltration membrane. As the main performance parameters, a suitable nanofiber membrane was selected to test its filtration performance. P/E-NCM with the ratio of 10/90 had a porosity of only 64%, so we did not do the water flux measurement with it. Figure 5 showed the water flux of P/E-NCM with the ratios of 20/80, 30/70, heat-treated 30/70, and 40/60 in 10 min at different operating pressures. It could be seen that the water flux of NCM increased with the increasing of pressure and decreased with prolonging test time at the same operating pressure, and decreased significantly at the high operating pressure. It was clearly presented in Figure 5(f) when the operating pressure were 0.025, 0.05, 0.075, 0.1, and 0.2 MPa, the average water flux of P/E (30/70)-NCM in 10 min were 880, 2555, 3141, 3795, and 5213 L/(m^2 h), respectively. Under the same condition, for P/E (30/70)-NCM, the average water flux were 629 2042, 2421, 2796, 4375 L/(m^2 h), respectively. For heat-treated P/E (30/70)-NCM, the average water flux were 589, 1854, 2098, 2511, 3955 L/(m^2 h), respectively. For P/E (40/60)-NCM, the average water flux were 683, 2123, 2523, 2810, 4533 L/(m^2 h), respectively. It probably caused by trapping impurities in membranes during the test process of water flux. As the filtration time extended, the impurity intercepted by nanofibers composite membrane increased gradually during the filtration process, leading to the water flux decreased slightly. However, with the increasing of operating pressure, the water flux of NCM increased. At the same time, impurities had a corresponding increase, resulting in water flux decreased more significantly with the extension of time at

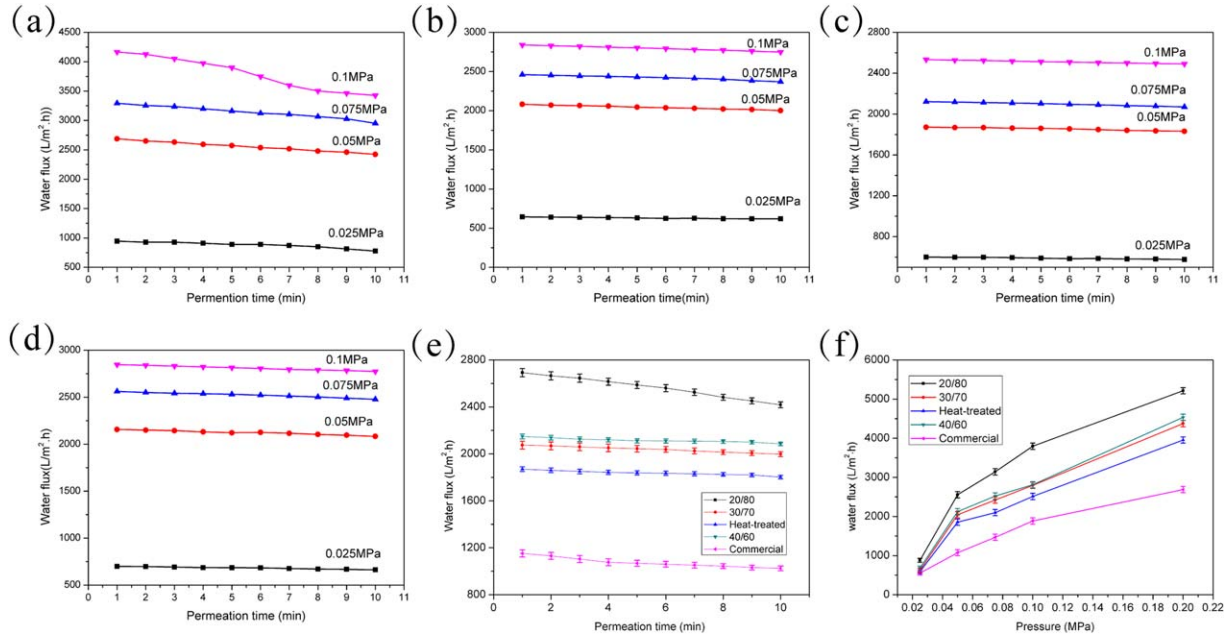

Figure 5. Time dependence of pure water flux under different pressures for P/E NCM with different blend ratios, (a) 20/80, (b) 30/70, (c) heat-treated 30/70, (d) 40/60, (e) Pure water flux of all kinds of membranes at the pressure of 0.05 MPa, and (f) pressure dependence of pure water flux for NCM. [Color figure can be viewed in the online issue, which is available at wileyonlinelibrary.com.]

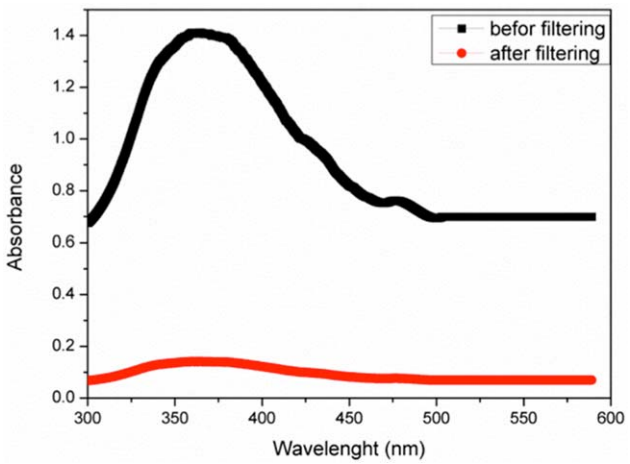

Figure 6. UV absorption spectrogram of TiO_2 suspension before and after filtering by P/E (30/70) NCM. [Color figure can be viewed in the online issue, which is available at wileyonlinelibrary.com.]

greater operating pressure. The results of NCM water flux were higher than the research before and the commercial cellulose ester microfiltration membrane.[36]

Figure 5(e) showed the water flux of NCM with four components ratio and commercial cellulose ester microfiltration membrane in 0.05 MPa operating pressure. With the increasing of filtration time, water flux attenuation of P/E (20/80)-NCM was seriously [Figure 5(e)]. The water flux of P/E (30/70)-NCM and P/E (40/60)-NCM had slightly difference due to their similar porosity. However, for heat-treated nanofiber membrane, the water flux was low because of its low porosity, what would affect the filtration performance. It was obviously that the water flux of NCM was much higher than the commercial cellulose ester microfiltration membrane, which was smaller than 1200 L/(m^2 h). Considering all the properties, P/E (30/70)-NCM was selected to do the following filtration performance test.

Filtration Performance

TiO_2 ultrafine powder is a kind of fine chemical products. In this study, TiO_2 (0.1–1 μm) suspension was used to evaluate filtration capability of P/E-NCM. The water flux device designed by ourselves was used to examine the rejection rate of the membrane to TiO_2 suspension.

Figure 6 showed UV absorption spectrogram of the TiO_2 suspension before and after filtration by P/E (30/70)-NCM filtration. As shown in Figure 6, the absorbance of TiO_2 suspension dropped seriously after filtration, and closed to 0.1. According to the eq. (2), the results revealed that the rejection rate of P/E (30/70)-NCM to TiO_2 suspension was above 95%. Therefore, P/E (30/70)-NCM was suggested for application in liquid microfiltration.

Membrane Fouling

In the process of membrane filtration, membrane fouling is a serious problem, which restricts its use in industry field due to the contamination and the shortened life expectancy of membranes by increasing filtration resistance. To study the membrane fouling, the TiO_2 suspension (0.5%) flux of P/E (30/70)-NCM was tested. Figure 7 showed the time dependence of TiO_2 suspension (0.5%) flux and total resistance of P/E (30/70)-NCM with the operation pressure was 0.05 MPa. As shown in Figure 7(a), the filtration process divided into two stages. In the initial stage of filtration, with the increasing of permeation time, the flux decreased rapidly due to the increasing of total membrane resistance, which was mainly caused by the adsorption and pore blocking of TiO_2 particles in membrane. However, with the extension of permeation time, the membrane resistance increased slightly, so the decreasing of flux became slower until the membrane filtration equilibrium. At 0.05 MPa operation pressure, the resulting P/E (30/70)-NCM possessed high flux [450.9 L/(m^2 h)] with rejection rate above 95%. Figure 7(b) showed the membrane resistance distribution of P/E (30/70)-NCM after the filtration process carried out in 60 min. As shown in the Figure 7(b), the total membrane filtration resistance R_t was composed of adsorption and pore blocking resistance R_{a+p} which was 34.4%, intrinsic membrane resistance R_m which was 21.3%, and cake deposition resistance R_c which was 44.3%. The data suggested that the membrane adsorption, membrane pore blocking resistance, and cake deposition resistance were the main reasons resulting in the water flux decline and the pollution

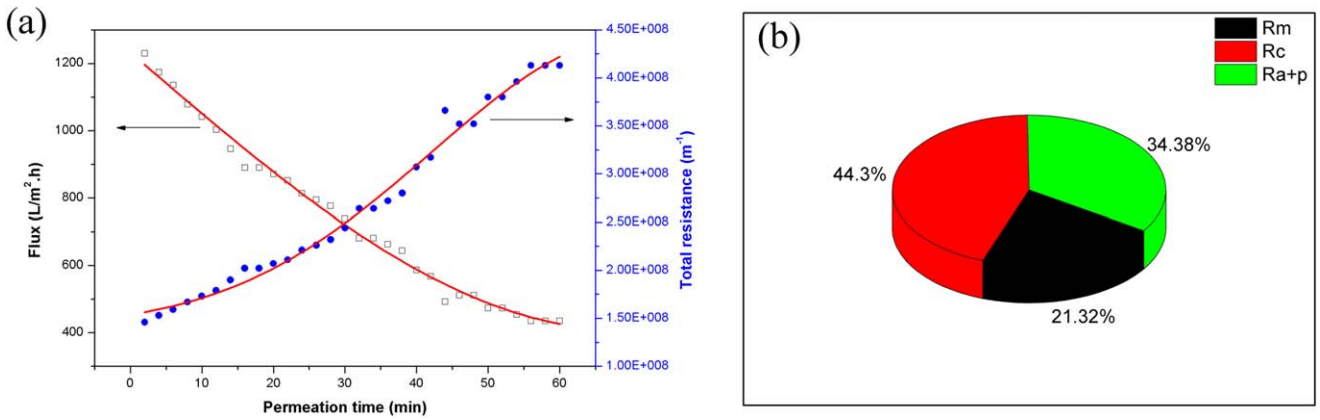

Figure 7. (a) Time dependence of TiO_2 suspension (0.5%) flux and total resistance of P/E (30/70) NCM. (b) Membrane resistance distribution of P/E (30/70) NCM after the filtration process in 60 min. [Color figure can be viewed in the online issue, which is available at wileyonlinelibrary.com.]

of the membrane, but intrinsic membrane resistance also could not be ignored. Therefore, methods should be adopted to avoid and eliminate this phenomenon in our further work.

CONCLUSIONS

High flux nanofibrous composite microfiltration membrane with low operation pressure for liquid filtration was fabricated in this contribution. The average diameter of EVOH fibers and PP fibers was 248 nm and 575 nm, and EVOH nanofibers had the specific surface area of 20.65 m^2/g. The mixing of PP and EVOH nanofibers combined both advantages, PP nanofibers as the scaffold played a supporting role, and EVOH nanofibers filled in the PP nanofibers network structure narrowed the pore size, improved the wettability, allowing the nanofibrous composite membrane to create fascinating features for liquid filtration. The porosity, water contact-angle, pore size of P/E-NCMM were bigger than EVOH nanofiber membranes. The P/E (30/70)-NCMM showed very high water flux [450.9 L/(m^2 h)] even at very low feeding pressure 0.05 MPa with above 95% retention for TiO_2 suspension. The results indicated that the combination of PP and EVOH nanofibers making nanofibrous composite microfiltration membrane a good candidate for liquid filtration.

ACKNOWLEDGMENTS

This research was supported by the National Natural Science Foundation of China (No. 21374015), and the program of Introducing Talents of Discipline to Universities (No. 111-2-04).

REFERENCES

1. Tamura, T.; Takemori, R.; Kawakami, H. *J. Power Sources* **2012**, *217*, 135.
2. Morcali, M. H.; Zeytuncu, B. *Int. J. Miner. Process.* **2015**, *137*, 52.
3. Yin, J.; Deng, B. *J. Membr. Sci.* **2015**, *479*, 256.
4. Josephson, J. *Environ. Sci. Technol.* **1984**, *18*, 375.
5. Fuenmayor, C. A.; Lemma, S. M.; Mannino, S.; Mimmo, T.; Scampicchio, M. *J. Food Eng.* **2014**, *122*, 110.
6. Miao, Y. E.; Zhu, G. N.; Hou, H.; Xia, Y. Y.; Liu, T. *J. Power Sources* **2013**, *226*, 82.
7. Liang, Y.; Cheng, S.; Zhao, J.; Zhang, C.; Sun, S.; Zhou, N.; Qiu, Y.; Zhang, X. *J. Power Sources* **2013**, *240*, 204.
8. Ayad, M. M.; Salahuddin, N. A.; Minisy, I. M.; Amer, W. A. *Sens. Actuators B Chem.* **2014**, *202*, 144.
9. Lamas-Ardisana, P. J.; Loaiza, O. A.; Anorga, L.; Jubete, E.; Borghei, M.; Ruiz, V.; Ochoteco, E.; Cabanero, G.; Grande, H. J. *Biosens. Bioelectron.* **2014**, *56*, 345.
10. Makaremi, M.; De Silva, R. T.; Pasbakhsh, P. *J. Phys. Chem. C* **2015**, *119*, 7949.
11. Choong, L. T.; Lin, Y. M.; Rutledge, G. C. *J. Membr. Sci.* **2015**, *486*, 229.
12. Arribas, P.; Khayet, M.; García-Payo, M. C.; Gil, L. *Sep. Purif. Technol.* **2014**, *138*, 118.
13. Jankovic, B.; Pelipenko, J.; Skarabot, M.; Musevic, I.; Kristl, J. *Int. J. Pharmaceut.* **2013**, *455*, 338.
14. Kampalanonwat, P.; Supaphol, P. *ACS Appl. Mater. Interfaces* **2010**, *2*, 3619.
15. Lu, Y.; Wu, Z.; Li, M.; Liu, Q.; Wang, D. *React. Funct. Polym.* **2014**, *82*, 98.
16. Zhao, Z.; Zheng, J.; Peng, B.; Li, Z.; Zhang, H.; Han, C. C. *J. Membr. Sci.* **2013**, *439*, 12.
17. Pereira, V. R.; Isloor, A. M.; Bhat, U. K.; Ismail, A. F. *Desalination* **2014**, *351*, 220.
18. Wang, X.; Fang, D.; Hsiao, B. S.; Chu, B. *J. Membr. Sci.* **2014**, *469*, 188.
19. Ding, B.; Kim, H. Y.; Lee, S. C.; Shao, C. L.; Lee, D. R.; Park, S. J.; Kwag, G. B.; Choi, K. J. *J. Polym. Sci. Polym. Phys.* **2002**, *40*, 1261.
20. Nayak, R.; Kyratzis, I. L.; Truong, Y. B.; Padhye, R.; Arnold, L.; Peeters, G.; O'Shea, M.; Nichols, L. *J. Mater. Sci.* **2012**, *48*, 273.
21. Sehaqui, H.; Ezekiel Mushi, N.; Morimune, S.; Salajkova, M.; Nishino, T.; Berglund, L. A. *ACS Appl. Mater. Interfaces* **2012**, *4*, 1043.
22. Sebe, I.; Szabo, B.; Nagy, Z. K.; Szabo, D.; Zsidai, L.; Kocsis, B.; Zelko, R. *Int. J. Pharmaceut.* **2013**, *458*, 99.
23. Hammami, M. A.; Krifa, M.; Harzallah, O. *J. Text. Inst.* **2014**, *105*, 637.
24. Lu, A.; Zhu, J.; Zhang, G.; Sun, G. *J. Mater. Chem.* **2011**, *21*, 18674.
25. Wang, H.; Xiao, R. *Polym. Adv. Technol.* **2012**, *23*, 508.
26. Wang, D.; Sun, G. *Eur. Polym. J.* **2007**, *43*, 3587.
27. Wang, D.; Sun, G.; Chiou, B. S. *Macromol. Mater. Eng.* **2007**, *292*, 407.
28. Wang, D.; Sun, G.; Yu, L. *Carbohydr. Polym.* **2011**, *83*, 1095.
29. Zhu, J.; Sun, G. *ACS Appl. Mater. Interfaces* **2014**, *6*, 925.
30. Liu, P.; Ouyang, Y.; Xiao, R. *J. Appl. Polym. Sci.* **2012**, *123*, 2859.
31. Zhu, M.; Xu, G.; Yu, M.; Liu, Y.; Xiao, R. *Polym. Adv. Technol.* **2012**, *23*, 247.
32. Ma, Z.; Kotaki, M.; Yong, T.; He, W.; Ramakrishna, S. *Biomaterials* **2005**, *26*, 2527.
33. Koehler, J. A.; Ulbricht, M.; Belfort, G. *Langmuir* **2000**, *16*, 10419.
34. Kim, E. S.; Liu, Y.; Gamal El-Din, M. *Environ. Sci. Technol.* **2012**, *46*, 2877.
35. Lee, W. *J. Membr. Sci.* **2003**, *216*, 217.
36. Li, M.; Wang, D.; Xiao, R.; Sun, G.; Zhao, Q.; Li, H. *Sep. Purif. Technol.* **2013**, *116*, 199.